Strong-Field Perspective on High-Harmonic Radiation from Bulk Solids

Takuya Higuchi, Mark I. Stockman, and Peter Hommelhoff

Phys. Rev. Lett. **113**, 213901 — Published 17 November 2014

DOI: 10.1103/PhysRevLett.113.213901

Strong-Field Perspective on High-Harmonic Radiation from Bulk Solids

Takuya Higuchi,[1,*] Mark I. Stockman,[2,3,4] and Peter Hommelhoff[1,2]

[1] *Department of Physics, Friedrich-Alexander-Universität Erlangen-Nürnberg, Staudstrasse 1, D-91058 Erlangen, Germany*
[2] *Max-Planck-Institut für Quantenoptik, Hans-Kopfermann-Strasse 1, D-85748 Garching, Germany*
[3] *Fakultät für Physik, Ludwig-Maximilians-Universität, Am Coulombwall 1, D-91058 Garching, Germany*
[4] *Department of Physics and Astronomy, Georgia State University, Atlanta, Georgia 30303, USA*

(Dated: September 4, 2014)

Mechanisms of high-harmonic generation from crystals are described by treating the electric field of a laser as a quasi-static strong field. Under the quasi-static electric field, electrons in periodic potentials form dressed states, known as Wannier-Stark states. The energy differences between the dressed states determine the frequencies of the radiation. The radiation yield is determined by the magnitudes of the inter-band and intra-band current matrix elements between the dressed states. The generation of attosecond pulses from solids is predicted. Ramifications for strong-field physics are discussed.

PACS numbers: 72.20.Ht, 42.65.Ky, 42.65.Re

Advances in intense pulsed lasers have opened up an avenue to field-induced non-perturbative nonlinear optical phenomena, such as high-harmonic generation (HHG) and attosecond pulse generation [1, 2]. The scope of these strong-field phenomena has been mainly focused on gaseous media, and was extended to solids recently [3–15]. In particular, HHG from wide-band-gap semiconductors under illumination of low-frequency laser has been reported [3, 4], which opened the door to extreme wavelength conversion employing condensed matters.

The non-perturbative character of the HHG manifests itself as plateau structures in its energy spectrum, which provide insights into the electronic dynamics on attosecond timescales. The HHG process of gases is well described by the three-step model: field ionization, acceleration, and recollision [16, 17]. The cutoff energy of the resultant radiation plateau is the sum of the ionization potential and the maximal kinetic energy gained by the electron during excursion, and thus scales quadratically with the laser field amplitude. In case of solids, however, this enlightening three-step model is not applicable, as is evidenced by the experimentally observed linear scaling of the cutoff energies to the field [3, 4].

To account for the mechanism of HHG from solids, several models have been proposed. (1) For example, Ghimire *et al.* considered the intraband current as the source of HHG [3, 18]. Due to the non-parabolicity of the conduction-band energy, the intraband current contains harmonics of the Bloch frequency $\Omega_{\mathrm{B}} \equiv qaE/\hbar$, where q is the unit charge, a is lattice constant of the crystal, and E is the electric field amplitude of the laser. This model explains the linear scaling of the cutoff energy with the laser field amplitude, but cannot treat the additional offset observed in the cutoff energy [3, 4]. (2) Another approach is to consider the inter-band polarization as the source [6–8]. In this model, highest-energy photons are emitted at the top of the bands: this gives the upper limit of the HHG energy, but does not explain the linear scaling.

These currently existing models cannot fully explain the experimentally observed scaling of the cut-off energy because inter- and intra-band light-matter interactions are considered separately. When the laser field is strong and the interaction is non-perturbative, the interplay between the inter- and intra-band contributions cannot be neglected, in analogue to breakdown of the rotating wave approximation for carrier-wave Rabi flopping in two-level systems [19–21]. The importance of avoiding this artificial separation for a proper prediction of the HHG radiation frequency is found in numerical simulations based on the integration of the time-dependent Schrödinger equation (TDSE) [7, 8, 13–15]. The validity of such a numerical approach is confirmed by its agreement with experiments [4]. Various proposals have been made based on the TDSE, for example to isolate an attosecond pulse by using two-color laser pulses [22]. These numerical simulations, however, require further interpretation of the results, and a more insightful way of determining the HHG cutoff energy has been eagerly demanded [6].

In this study, we propose a semi-analytical model to gain insight into the physical processes involved in the generation of HHG radiation in solids, and to understand the experimentally observed cutoff energies. The essential point of our model is to consider electronic states dressed with a quasi static electric field via both inter- and intra-band couplings, which are known as Wannier-Stark (WS) localised states [10, 11, 23]. The energy spectrum and the wave functions of these dressed states determine the radiation energy and yield of the HHG. We show that the highest energy photons from solids are emitted when the laser field peaks, which suggests participation of the adiabatic WS states. Based on this understanding, we predict the possibility of generation of isolated attosecond pulses from solids.

Electrons in a periodic lattice interact with the optical electric field through inter-band and intra-band cou-

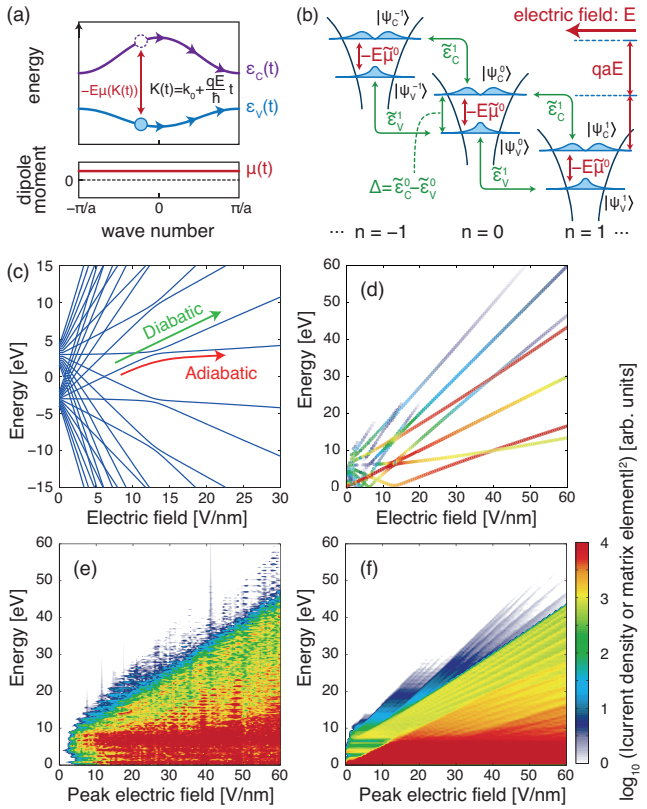

FIG. 1: (Color) (a) Schematic of the dynamics of electrons in the valence and conduction bands. The electron experiences both inter-band transition and the intra-band acceleration. (b) Coordinate-space representation of the system under a static electric field. (c) Quasi-energy spectra as functions of the quasi-static electric field. (d) Energy spectra of the radiation as functions of the quasi-static electric field. The color shows the intensity amplitude of the current matrix elements. (e) Numerically obtained current density spectra as functions of the peak electric field of the incident laser pulse. (f) Integrated values of the intensity amplitude of the current matrix elements in (d) over the same laser waveform as in (e).

plings, which are found in the Schrödinger equation for semiconductors [4, 13, 21]:

$$\mathcal{H}(t) = \int_0^{\frac{2\pi}{a}} dk \Big[\sum_\lambda \varepsilon_\lambda(k) \hat{a}^\dagger_{\lambda,k} \hat{a}_{\lambda,k} - E(t) \Big[\sum_{\lambda,\lambda'} \mu_{\lambda\lambda'}(k) \hat{a}^\dagger_{\lambda,k} \hat{a}_{\lambda',k} + iq \sum_\lambda \hat{a}^\dagger_{\lambda,k} \nabla_k \hat{a}_{\lambda,k} \Big] \Big] \quad (1)$$

Here $\hat{a}_{\lambda,k}$ is the annihilation operator of an electron with a wavenumber k, the indices λ and λ' label the bands. $\varepsilon_\lambda(k)$ is the electron energy of band λ at k, $\mu_{\lambda\lambda'}(k)$ is the inter-band dipole moment between the bands λ and λ' at k. The three terms describe the energies of the band electrons, the inter-band polarization, and the intra-band polarization, respectively.

Higher-harmonic radiation oscillates much faster than the laser field. Also, we assume the driving-laser frequency to be much smaller than the band gap divided by $\hbar$ so that the material is transparent to the laser. Therefore, we assume that the laser electric field is quasi-static, $E(t) = E_0$, and watch the electronic states under this assumption. The last term in Eq. (1) results in the intra-band accleration of the electrons: $K(t) = k_0 + \frac{qE}{\hbar}t$, where k_0 is the initial wave number [Fig. 1(a)]. The electron-electron interaction works as pure dephasing at the time scale of tens of femtoseconds [21], so the dynamics of the electrons with different k_0 can be independently calculated. We take an interaction-representation picture for k so that $k = K(t)$ changes in time following this intra-band acceleration, so the last term in Eq. (1) is eliminated. The cost we pay is that the Hamiltonian now depends on time even though we assumed a static electric field. This temporal dependence is periodic in time, hence we can employ the Floquet theorem to obtain the solutions.

We illustrate how to apply the Floquet method using a one-dimensional two-band model for example, i.e., conduction band and valence band (λ = C or V, respectively). Note that this procedure is applicable to any number of bands. In matrix form, the Hamiltonian is

$$H(t) = \begin{bmatrix} \varepsilon_{\rm V}(K(t)) & -E_0\mu(K(t)) \\ -E_0\mu^*(K(t)) & \varepsilon_{\rm C}(K(t)) \end{bmatrix}. \quad (2)$$

The conduction- and valence-band energies and the dipole coupling energies are periodic functions of k. Under a static field, this periodicity is imprinted onto temporal periodicity because $K(t) = k_0 + \frac{qE}{\hbar}t$ is linear to t. Therefore, the Hamiltonian is also periodic in time, and can be decomposed into a Fourier series as

$$H(t) = \sum_n e^{-in\Omega_{\rm B}t} \tilde{H}^n, \quad \tilde{H}^n \equiv \begin{bmatrix} \tilde{\varepsilon}^n_{\rm V} & -E_0\tilde{\mu}^n \\ -E_0\tilde{\mu}^{n*} & \tilde{\varepsilon}^n_{\rm C} \end{bmatrix}. \quad (3)$$

where $\Omega_{\rm B} = aeE_0/\hbar$ is the frequency of the periodicity, which is the Bloch frequency. $\tilde{\mu}^n$ and $\tilde{\varepsilon}^n_\lambda$ are the Fourier coefficients of $\mu(K(t))$ and $\varepsilon_\lambda(K(t))$, respectively.

We can now apply the Floquet theorem to this system. The problem to find solutions of the original Schrödinger equation (2) is translated into solving the following eigenvalue problem [24]: $\sum_{\nu',n'} \left(H^{n-n'}_{\nu\nu'} - n\hbar\Omega_{\rm B}\delta_{\nu\nu'}\delta^{nn'} \right) |\phi^{n'}_{\nu'}\rangle = \epsilon^n_\nu |\phi^n_\nu\rangle$. ϵ^n_ν is a quasi-energy, and the eigenstate $|\phi^n_\nu\rangle$ is a WS state [25]. Here the indices ν and ν' labels different Floquet quasi-energy series. Within one series, the quasi-energies are equidistant : $\epsilon^n_\nu - \epsilon^{n'}_\nu = \hbar(n-n')\Omega_{\rm B}$. The number of the series is the same as the number of the original electronic bands. The solutions of the original Schrödinger equation are constructed from the quasi-energy eigenstates of the Floquet Hamiltonian:

$$|\Psi(t)\rangle = \sum_\nu \sum_n C_\nu e^{-i\frac{\epsilon^n_\nu}{\hbar}t} |\phi^n_\nu\rangle . \quad (4)$$

The linear-combination coefficients C_ν are determined by the initial electron states and the prior temporal evolution of the field, following the Landau-Zener tunnelling probability [5, 10, 26, 27]

It is interesting to see that the above procedure of the Floquet method can be mapped into a coordinate-space picture via a standard tight-binding procedure [Fig. 1(b)]. Consider atomic Wannier states $|\phi_\lambda^n\rangle$ in a lattice, where n labels the site position and λ is the band index. $\tilde{\varepsilon}_\lambda^n$ corresponds to the coupling to the n-th neighbor site. Diagonalization of the Hamiltonian without field gives the standard band structure. An external electric field provides two additional effects. The first is the position(x)-dependent potential energy shift, $-qxE$. The second is the inter-band mixing between the n-th neighbors via dipole coupling $\tilde{\mu}^n$. Diagonalization of this coordinate-space Hamiltonian gives the same energy spectrum as the Floquet quasi-energy spectrum.

Figure 1(c) shows the quasi-energy spectra as function of the quasi-static field amplitude. Parameters are chosen to simulate a typical wide-band-gap semiconductor: a band offset $\Delta \equiv \tilde{\varepsilon}_{\rm C}^0 - \tilde{\varepsilon}_{\rm V}^0$ of 6 eV, a conduction-band width $2\tilde{\varepsilon}_{\rm C}^1 = 2\tilde{\varepsilon}_{\rm C}^{-1}$ of 3 eV, a valence-band width $2\tilde{\varepsilon}_{\rm V}^1 = 2\tilde{\varepsilon}_{\rm V}^{-1}$ of 2 eV, and an intra-atomic dipole moment $\tilde{\mu}^0$ of 0.1 $|e^-|\cdot$nm. The other parameters ($\tilde{\varepsilon}_\lambda^n$ for $|n| \geq 2$ and $\tilde{\mu}^n$ for $|n| \geq 1$) are zero. For the diagonalization, we introduced a cutoff in n as $|n| \leq 7$. Increasing the cutoff does not change the quasi-energies of the $n = 0$ states for $\Omega_{\rm B} > \Delta$ (i.e., $|E| > \Delta/qa$) because the mixing between wave functions having a large difference in n is negligibly small. In the coordinate space picture [Fig. 1(b)], this corresponds to neglecting the inter-atomic coupling if they are separated by na, which is larger than the WS localization length [10].

Next, we calculate the current. The intra-band current operator is obtained from the electron group velocity as $J_{\lambda\lambda'}(t) = \frac{e}{\hbar}\frac{\partial \varepsilon_\lambda(k)}{\partial k}\Big|_{k=K(t)} \delta_{\lambda\lambda'}$. The inter-band current is given as the temporal derivative of the interband polarization $P_{\lambda\lambda'}(t) = \mu_{\lambda\lambda'}(K(t))$. Both are periodic in time, and thus can be described using their Floquet Matrix elements. We calculate the expectation value of the total current for the dressed electronic state in Eq. (4):

$$\frac{d}{dt}\langle P(t)\rangle + \langle J(t)\rangle = \sum_{\nu,\nu'}\sum_{n,n'} C_\nu^* C_{\nu'} e^{i\frac{\epsilon_\nu^n - \epsilon_{\nu'}^{n'}}{\hbar}t} \times \left(\langle \phi_\nu^n | P_{\rm F} | \phi_{\nu'}^{n'} \rangle \frac{i(\epsilon_\nu^n - \epsilon_{\nu'}^{n'})}{\hbar} + \langle \phi_\nu^n | J_{\rm F} | \phi_{\nu'}^{n'} \rangle \right). \quad (5)$$

Here, the Floquet matrix $P_{\rm F}$ is defined as $\langle \psi_\lambda^n | P_{\rm F} | \psi_{\lambda'}^{n'} \rangle \equiv \langle \psi_\lambda | \tilde{P}^{(n-n')} | \psi_{\lambda'} \rangle$, where $|\psi_\lambda^n\rangle \equiv \exp(-in\Omega_{\rm B}t)|\psi_\lambda\rangle$ are the bases in the extended Hilbert space and $|\psi_\lambda\rangle$ are the bases of the original equation (2). $J_{\rm F}$ is defined similarly. See supplementary information for details.

The oscillating total current in Eq. (5) works as the source of radiation. The difference between quasi-energies, $\varepsilon_\nu^n - \varepsilon_{\nu'}^{n'}$, gives the photon energy of the radiation. The radiation yield is determined by the terms in parenthesis in Eq. (5), i.e., the matrix element of the total current operator between different quasi-energy states. Figure 1(d) shows the energy spectra of the current, with the intensity amplitudes of the current matrix elements encoded in color. According to the quasi-energy spectrum, seemingly infinitely high energy photons can be emitted because the quasi-energy spreads over infinite values. However, this is not the case because the current matrix elements between different quasi-energy eigenstates steeply drops in logarithmic scale as the quasi-energy difference increases. The coefficients C_ν has a secondary influence to the radiation power because the population distribution changes within linear scale, as we will see later. Note that propagation effects modify the HHG spectra from the current spectra through absorption and phase mismatch [18].

In a strong-field limit, i.e., $\hbar\Omega_{\rm B} > \Delta$, the quasi-energies are approximated as $\epsilon_{(\pm)}^n \approx n\hbar\Omega_{\rm B} \pm \sqrt{(\Delta/2)^2 + (\hbar\Omega_{\rm R})^2} + (\tilde{\varepsilon}_{\rm C}^0 + \tilde{\varepsilon}_{\rm V}^0)/2$. Here $\Omega_{\rm R} \equiv E\tilde{\mu}^0$ is the Rabi frequency between the two Wannier states within a single atomic site, and the term including $\Omega_{\rm R}$ corresponds to Stark shift. The difference between two quasi-energy states gives the radiation energy:

$$\epsilon_{(+)}^n - \epsilon_{(-)}^{n-N} \approx N\hbar\Omega_{\rm B} + \sqrt{\Delta^2 + (2\hbar\Omega_{\rm R})^2}. \quad (6)$$

When $\Omega_{\rm R} \ll \Delta$, this value converges to $N\Omega_{\rm B} + \Delta$. This means that the cut-off energy is linear to the field amplitude because a multiple of the Bloch frequency $N\hbar\Omega_{\rm B}$ is included. On top, Δ remains as an offset, which accounts for the experimentally obtained offset in the cutoff energy [3, 4]. Note that in the carrier-wave Rabi flopping regime ($\Omega_{\rm R} \gg \Delta$), the cutoff is $N\Omega_{\rm B} + 2\Omega_R$.

To show the validity of this picture, we compare it with numerical results [Fig. 1(e)]. The temporal evolution of the TDSE is obtained with the Crank-Nikolson method [28]. The valence band is initially fully occupied, while the conduction band is empty. We calculate the total current density $|\frac{d}{dt}\langle P(t)\rangle + \langle J(t)\rangle|^2$. The laser pulse has a central frequency of 200 THz and a FWHM of the intensity envelope of 30 fs. We changed the peak electric field in the simulations, while fixing the waveform. Carrier-envelope-phase variation induces negligible change in HHG spectra for such relatively long pulses. In comparison, we integrated the radiation yield in Fig. 1(d) over the laser waveform to estimate the radiation spectra [Fig. 1(f)]. Quantitative agreement between the numerical and the semi-analytical results is found. For example, several cutoff steps in the energy (change in color) are observed in the two pictures, overlapping each other. Hence, the semi-analytical results are well supported by numerical simulations. They deviate when $|E| < \Delta/qa$, because the quasi-static assumption is only

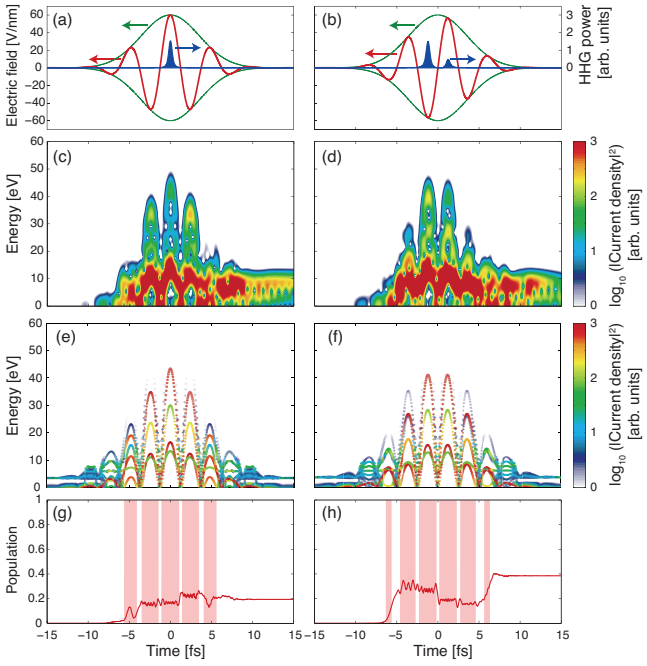

FIG. 2: (Color) Prediction of the possible generation of attosecond pulse. The incident laser waveforms having (a) cosine and (b) sine wave forms are plotted as the red curves, while their envelopes (green curves) are identical. The blue shaded areas show the power of the HHG through high-pass filters, having cutoff energies at (a) 40 eV and (b) 38 eV. (c)(d) Numerically obtained HHG spectrograms. The window function is a gaussian having a FWHM of 0.67 fs, i.e., 6.2 eV in energy, which broadens the spectrograms. (e)(f) Spectra of the total current matrix elements as functions of time. The color indicates the intensity amplitude of the matrix elements. (g)(h) Temporal evolution of the upper-level population. The shaded areas indicate $|\hbar\Omega_{\rm B}| > \Delta$, indicating the field amplitude exceeds the last anti-crossing in Fig. 1(b).

valid for stronger field values. Note that the computation cost for the semi-analytical method was three orders of magnitude smaller than that of the numerical integration.

So far we have clarified the mechanisms of HHG based on quasi-static electronic states. This provides us an opportunity to predict the possibility of generation of isolated attosecond pulse(s), whose waveforms can be controlled by the carrier-envelope phase (CEP) of the incident laser pulse. Figures 2(a) and (b) show two laser waveforms having different (0 and $\pi/2$) CEPs, which correspond to cosine and sine waveforms, respectively. We numerically simulate the temporal evolution of the TDSE under these laser waveforms, and obtain spectrograms of the currents [Figs. 2(c) and (d)]. These spectrograms show notable differences: the cosine pulse generates a single high-energy peak while the sine pulse generates a double peak. Single or double attosecond pulses can be separated from the rest of the radiation by introducing high-pass filters [Figs. 2(a) and (b)].

The quasi-static assumption insightfully accounts for the main features in the spectrograms when $|E| > \Delta/qa$. Figures 2 (e) and (f) show the energy and the yield of the radiation under the quasi-static field approximation, which well explains the photon energies of the radiation peaks in Figs. 2(c) and (d). Note that there remains a considerable radiation at low energies in the spectrogram after the laser pulse passes. This cannot be treated in the quasi-static field model because it is applicable when $|E| > \Delta/qa$.

One limitation of the present approach is that the coefficients C_ν in Eq. (4) cannot be determined with the present value of the field alone, because they are determined by the initial conditions and depend on how the field evolved. So, it is worth considering how these coefficients evolve in the numerical simulations. The speed of the change in the field value determines the tunnelling rate when the field value goes through anti-crossings in the quasi-energy spectra. For example, the last anti-crossing in Fig. 1(c) is $\sim$ 0.5 eV wide (i.e., the one for the largest field amplitude), which is comparable to the frequency of the laser field, 0.83 eV/$\hbar$. Therefore, when the field value goes across the anti-crossings, electrons experience intermediate transitions between adiabatic and diabatic ones through Landau-Zener tunnelling [5, 10, 26, 27]. This is found in Figs. 2 (g) and (h), showing the populations of an upper energy Wannier state. This temporal evolution of the populations accounts for the more detailed features in the HHG spectrograms. For example, the two high-energy pulses in Fig. 2(d) have different intensities, and this difference reflects the difference in upper-level population in Fig. 2(h). The evolution of the upper-state population is important to understand other strong-field phenomena, such as laser-field induced currents in dielectrics [5]. The present picture can bridge the gap between these intriguing phenomena.

In this Letter, we treat a one-dimensional model because of its universal and heuristic insight. In particular, Eq. (6) explains why the cutoff energy scales linearly to the field amplitude with an offset. The present method is fundamentally applicable to the three-dimensional (3D) models by means of many-mode Floquet theory [29]. However, a 3D model cannot be equally universal because there are many crystallographic classes; the direction of the field with respect to crystallographic lattice is another important factor [4, 8]. Therefore, the 3D computations should be done for specific crystals and optical polarizations. These extensions to higher dimensions will be published else where.

To summarise, the HHG radiation mechanism in solids is described as radiation from localised WS states in the strong-field regime, $|E| > \Delta/qa$. The differences of the quasi-energies of the WS states determine the radiation energies. The current matrix elements between different quasi-energy states determine the radiation yields.

This mechanism is analogous to the one employed in the quantum cascade laser, where the mini-bands are formed in semiconductor superlattices under a static field, and the radiation frequency corresponds to the energy difference between mini-bands [30, 31]. In this sense, HHG in solids can be considered as quantum-cascade emission at extreme ultraviolet frequencies, where high-energy carriers are coherently injected through Landau-Zener tunnelling. Highest energy radiation is emitted when the incident field peaks. This greatly differs from the atomic case, where the recollision event of the electrons with highest kinetic energy does not happen at the time when the laser field peaks.

The authors acknowledge S. C. Furuya for helpful discussions. This work was supported by the DFG Cluster of Excellence Munich-Centre for Advanced Photonics and ERC grant "Near Field Atto." TH acknowledges support by JSPS postdoctoral fellowship for research abroad. Major funding for MIS was provided by Grant No. DE-FG02-01ER15213 from the Chemical Sciences, Biosciences and Geosciences Division. Supplementary funding came from Grant No. DE-FG02-11ER46789 from the Materials Sciences and Engineering Division of the Office of the Basic Energy Sciences, Office of Science, U.S. Department of Energy, Grant MURI No. N00014-13-1-0649 from the US Office of Naval Research.

* E-mail: takuya.higuchi@fau.de

[1] P. B. Corkum and F. Krausz, Nat Phys **3**, 381 (2007).
[2] F. Krausz and M. Ivanov, Rev. Mod. Phys. **81**, 163 (2009).
[3] S. Ghimire, A. D. DiChiara, E. Sistrunk, P. Agostini, L. F. DiMauro, and D. A. Reis, Nat Phys **7**, 138 (2011).
[4] O. Schubert, M. Hohenleutner, F. Langer, B. Urbanek, C. Lange, U. Huttner, D. Golde, T. Meier, M. Kira, S. W. Koch, and R. Huber, Nat Photon **8**, 119 (2014).
[5] A. Schiffrin, T. Paasch-Colberg, N. Karpowicz, V. Apalkov, D. Gerster, S. Muhlbrandt, M. Korbman, J. Reichert, M. Schultze, S. Holzner, J. V. Barth, R. Kienberger, R. Ernstorfer, V. S. Yakovlev, M. I. Stockman, and F. Krausz, Nature **493**, 70 (2013).
[6] M. Ivanov and O. Smirnova, Chem. Phys. **414**, 3 (2013).
[7] G. Vampa, C. R. McDonald, G. Orlando, D. D. Klug, P. B. Corkum, and T. Brabec, in *Frontiers in Optics 2013 Postdeadline* (OSA, Florida, USA, 2013), p. FW6C.4.
[8] G. Vampa, C. R. McDonald, G. Orlando, D. D. Klug, P. B. Corkum, and T. Brabec, Phys. Rev. Lett. **113**, 073901 (2014).
[9] F. Krausz and M. I. Stockman, Nat. Photon. **8**, 205 (2014).
[10] M. Durach, A. Rusina, M. F. Kling, and M. I. Stockman, Phys. Rev. Lett. **105**, 086803 (2010).
[11] M. Durach, A. Rusina, M. F. Kling, and M. I. Stockman, Phys. Rev. Lett. **107**, 086602 (2011).
[12] S. Y. Kruchinin, M. Korbman, and V. S. Yakovlev, Phys. Rev. B **87**, 115201 (2013).
[13] D. Golde, T. Meier, and S. W. Koch, Phys. Rev. B **77**, 075330 (2008).
[14] A. F. Kemper, B. Moritz, J. K. Freericks, and T. P. Devereaux, New J. Phys. **15**, 023003 (2013).
[15] M. Korbman, S. Y. Kruchinin, and V. S. Yakovlev, New Journal of Physics **15**, 013006 (2013).
[16] P. B. Corkum, Phys. Rev. Lett. **71**, 1994 (1993).
[17] M. Lewenstein, P. Balcou, M. Y. Ivanov, A. L'Huillier, and P. B. Corkum, Phys. Rev. A **49**, 2117 (1994).
[18] S. Ghimire, A. D. DiChiara, E. Sistrunk, G. Ndabashimiye, U. B. Szafruga, A. Mohammad, P. Agostini, L. F. DiMauro, and D. A. Reis, Phys. Rev. A **85**, 043836 (2012).
[19] L. Plaja and L. Roso-Franco, J. Opt. Soc. Am. B **9**, 2210 (1992).
[20] S. Hughes, Phys. Rev. A **62**, 055401 (2000).
[21] D. Golde, T. Meier, and S. W. Koch, J. Opt. Soc. Am. B **23**, 2559 (2006).
[22] O. D. Mücke, Phys. Rev. B **84**, 081202 (2011).
[23] D. Emin and C. F. Hart, Phys. Rev. B **36**, 7353 (1987).
[24] S.-I. Chu and D. A. Telnov, Phys. Rep. **390**, 1 (2004).
[25] M. Glück, A. Kolovsky, H. Korsch, and N. Moiseyev, Eur. Phys. J. D **4**, 239 (1998).
[26] L. Landau, Phys. Z. Sowjetunion **2**, 46 (1932).
[27] C. Zener, Proc. R. Soc. A **137**, 696 (1932).
[28] J. Crank and P. Nicolson, Proc. Camb. Phil. Soc. **43**, 50 (1947).
[29] T. S. Ho, S. I. Chu, and J. V. Tietz, Chem. Phys. Lett. **96**, 464 (1983).
[30] J. Faist, F. Capasso, D. L. Sivco, C. Sirtori, A. L. Hutchinson, and A. Y. Cho, Science **264**, 553 (1994).
[31] B. S. Williams, Nat Photon **1**, 517 (2007).